Don't refer to "optimal" anywhere in abstract (& probably shouldn't). Is there a better word?

process vs model vs framework. I suggest "model" and "approach". Be consistent.

Optimising Energy Storage Size in Energy-Harvesting Intermittent Computing Systems

Jie Zhan, Alex S. Weddell, *Member, IEEE,* and Geoff V. Merrett, *Member, IEEE*

***Abstract*—Batteryless energy-harvesting devices are promising for a sustainable IoT. Forward progress in such devices is maintained by intermittent computing, where volatile computing state is saved into and restored from nonvolatile memory before and after power failures. Current intermittent computing approaches typically minimise energy storage to reduce device dimensions and recharging time. However, minimising energy storage results in expensive state-saving and -restoring overheads and impedes forward progress, whereas increasing energy storage requires more space and longer recharging time. In this paper, we propose a model-based process of identifying the proper energy storage capacity which trades off forward progress, dimensions, and recharging time. We develop a theoretical intermittent computing model to define the relationship between forward progress and energy storage capacity. Using this model, we show that sizing energy storage capacity can improve forward progress by up to 64.9 %. The model is experimentally validated based on an MSP430FR6989 microcontroller, showing high accuracy of 0.5 % mean absolute percentage error. Finally, we integrate the model into a photovoltaic-based energy-harvesting device framework to demonstrate the sizing process given various real-world light source datasets.**

***Index Terms*—Intermittent computing, energy harvesting, energy storage, forward progress, batteryless, wireless sensor networks, internet of things.**

I. Introduction

INTERNET of Things (IoT) devices are becoming ubiquitous, with tens of billions of devices to be installed in possibly hard-to-reach locations [1]–[4]. Conventionally, these devices are battery-powered, and thus have constrained lifespan and require impractical replacement work. To circumvent the limited battery lifespan, energy-harvesting IoT devices becomes a solution.

Environmentally harvested power is intrinsically variable and intermittent [5]. Traditionally, large energy storage in forms of rechargeable batteries or supercapacitors, is adopted to buffer the variable harvested power and provide a reliable power supply [6]–[11]. Unfortunately, such types of energy storage may raise pollution concerns, increase cost and device dimensions, and still have limited lifespan, yet using an energy-harvesting supply without energy buffering hinders execution by frequent power failures.

Recently, *intermittent computing* has been developed in research with the aim of removing large energy storage while maintaining execution despite frequent power failures [12]–[17]. During active periods, intermittent computing systems save system volatile computing state, e.g. CPU register data, RAM data, into nonvolatile memory (NVM) either at pre-installed points (*static methods*) or when the supply is about to fail (*reactive methods*) [18], [19]. In intermittent computing, *forward progress* denotes the effective program progress, excluding re-executed progress, lost progress, and state-saving and -restoring operations [20], [21]. The amount of forward progress directly determines application performance, e.g. program iteration rate or task completion time. We describe forward progress as *the ratio of the effective execution time to the total time*, without being restricted to a specific workload.

Current intermittent computing approaches typically adopt only a minimum amount of energy storage, which is just enough for the most energy-expensive atomic operation[1] with the goal of minimising device dimensions and recharging time [13], [14], [22]–[26]. However, in exploration we found that a device with minimum energy storage has to frequently go through the cycle of: wake up, restore state, execute code, save state, and halt, thereby consuming much energy in saving and restoring operations. Provisioning more energy storage prolongs the operating cycles and reduces the frequency of state saving and restoring operations, and hence, improves forward progress. However, larger energy storage also increases leakage current, occupies more space, and requires longer recharging time. The relationship between energy storage capacity and forward progress remains unexplored. Also, how to size energy storage to improve forward progress while balancing the physical size and recharging time is still a challenge.

In this paper, we provide a model-based sizing process of energy storage in intermittent computing, which improves forward progress and balances capacitor volume and recharging time. In summary, the main contributions of this paper are:

- A model-based sizing process that identifies the optimal energy storage capacity in deploying energy-harvesting intermittent computing (EHIC) devices, which trades off forward progress, capacitor volume, and recharging time (Section III).
- A theoretical model of reactive intermittent computing to estimate forward progress (Section IV) which is experimentally validated with only 0.5 % mean absolute percentage error (MAPE) (Section VI).
- An exploration based on the model, where we analyse the energy storage sizing effect on forward progress with

4 contributions very wordy, and I have trouble following them (especially 3 & 4).

Can you guarantee optimality? (see *, too)

The authors are with School of Electronics and Computer Science, University of Southampton, Southampton, SO17 1BJ, UK.

Software of this work will be open-source upon acceptance of this paper.

[1] Atomic operations in intermittent computing denote operations that should be completed in one continuous period. If an atomic operation is interrupted by a power failure, it should be re-executed rather than resumed. Examples of atomic operations include saving and restoring volatile state, transmitting and receiving packets, and sampling sensors.

I think you need to present 2 before 1?

compared to what? (could be infinite surely?

respect to supply current and volatile state size, showing up to 64.9 % forward progress improvement (Section V).

- A demonstration of the sizing process with the theoretical model integrated into a photovoltaic-based (PV-based) EHIC system model under various real-world light source datasets, where the suggested capacity achieves 98.3 % of the maximum forward progress while saves 71.7 % capacitor volume and 83.8 % recharging time (Section VII).

gvm 02/March/20.

II. Background and Related Work

A. Intermittent Computing

Intermittent computing aims at maintaining progress despite frequent power failures and insufficient power supply, such that the devices can operate even directly powered by energy harvesters. The basic mechanism is to back up volatile computing state (lost if the supply fails) as nonvolatile state (preserved if the supply fails) during active periods; when the supply recovers, the lost volatile state is restored from the saved nonvolatile state to resume execution. Approaches in intermittent computing can be classified as *static* and *reactive*.

1) Static Intermittent Computing: Static approaches save volatile state into NVM at design-time or compile-time preinstalled points, either by inserting checkpoints or decomposing a program into atomic tasks. After power failures, the progress rolls back and resumes from the last saved checkpoint or task boundary. Advantages in static approaches include eliminating additional hardware and ensuring operation atomicity. However, the rollback of progress intrinsically introduces issues on memory consistency code re-execution and wastes energy on lost and re-executed progress. Also, if the consumption between two successive checkpoints or task boundaries exceeds the amount that the energy storage can guarantee, the progress may never proceed due to insufficient power input.

2) Reactive Intermittent Computing: In contrast to static approaches, reactive approaches save volatile state in NVM when supply is about to fail by monitoring supply voltage. Specifically, reactive intermittent computing saves volatile state and enters a low-power mode (execution halted) if supply voltage falls below a save threshold. This save threshold should be set high enough to successfully save volatile state before power fails. By entering the low-power mode, reactive approaches avoid re-execution, and hence, typically make more forward progress than static approaches. In a comparison between static [27] and reactive [13] approaches, the reactive approach achieves a 2.5× mean speedup in computational workloads [28]. Therefore, we focus on reactive intermittent computing approaches in this work.

B. Modelling Intermittent Computing

A few models about intermittent computing have been proposed to explore design space. Su et al. [29] provide a model to explore the impact of sizing energy harvester and energy storage on a dual-channel solar-powered nonvolatile sensor node, but their exploring range of supercapacitors spans from 10F to 10^4F, which is significantly larger than a typical scale of energy storage (µF to mF scale) in intermittent computing. EH model [30], [31] explores forward progress with different parameter settings in intermittent computing, but the model only considers a single active period without considering inactive periods that scale down the effective forward progress, and hence, the model cannot predict the effective forward progress. Jackson et al. [32] also present a modelling approach to explore energy storage effect, where they suggest that novel batteries are preferable in order to offer reliable task completion and to improve energy utilization. However, they do not provide guidance on how to design energy storage, and their model lacks a detailed state-saving and -restoring mechanism in intermittent computing.

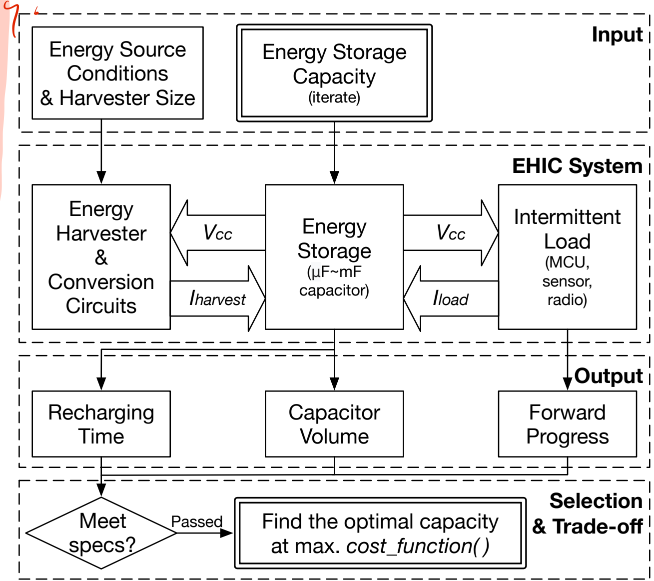

Fig. 1. Overview of energy storage sizing process and EHIC system.

III. Sizing Process of Energy Storage

A. Overview

The proposed sizing process aims at identifying the optimal energy storage capacity that improves forward progress and balances the side effects, i.e. increased dimensions and recharging time. Essentially, the sizing process inputs a range of energy storage capacities into an EHIC system model to get forward progress, capacitor volume, and recharging time, and trades off them in a cost function to obtain the optimal energy storage capacity. This process is summarised in Fig. 1 with details explained as follows:

- **Input**: An expected time trace of energy source conditions should be collected at the location of deployment. Assuming the energy source is equally distributed in the deployed space, scaling the energy harvester size changes the scale of harvested power.
- **EHIC System and Output:** This is an EHIC system model which simulates with the energy source trace and outputs forward progress, capacitor volume, and recharging time. We provide a framework to configure this system model (explained in Section III-B).
- **Selection and Trade-off**: Evaluate the optimal capacity by balancing forward progress and the side effects on

capacitor volume and recharging time in a cost function. We provide a cost function in Equation (1) as an example:

$$f = \frac{\alpha_{exe}}{k_1} - (\frac{v_{cap}}{k_2})^2 - (\frac{T_{recharge}}{k_3})^2 \tag{1}$$

where v_{cap} represents capacitor volume and $T_{recharge}$ represents recharging time. k_1, k_2, and k_3 are linear scalers, which are empirically determined according to design specifications. The negative side effects are calculated in quadratic forms so as to punish high values more heavily. We only consider the above three factors in this paper to size energy storage, but other factors can also be included, e.g. dimensions of energy harvesters.

B. EHIC System Framework

This framework provides a guide to construct an EHIC system model that estimates forward progress of EHIC devices in real-world deployment. A configured model according to this framework is then used to explore the effect of energy storage capacity on forward progress.

The EHIC system framework is shown as a part in Fig. 1. The model is driven by energy source conditions as a function of time. The framework divides the system into three modules, i.e. *Energy Harvester and Conversion Circuits*, *Energy Storage*, and *Load*. The three modules communicate by their voltage and current flows. Due to the variety in each module, the three module should be individually specified to represent the target platform according to the techniques implemented.

1) Energy Harvester and Conversion Circuits: The energy harvester module transduces energy source conditions into electrical power. Typically, the power harvested from the energy harvester should be conditioned to provide a suitable voltage for charging the energy storage and supplying the load efficiently. However, in intermittent computing, such conversion circuits may be removed to increase power efficiency, using only a diode to prevent current backflow. The energy harvester and conversion circuits can be modelled together as a module because they are usually coupled and integrated.

2) Energy Storage: Energy storage in EHIC devices is usually in the form of a µF- to mF-scale capacitor. The energy storage provides the minimum length of an execution period, which should be enough to complete the most energy-expensive atomic operation.

3) Intermittent Load: The load module includes all the power consumers in an EHIC device, such as a microcontroller, sensors, and a radio. As mentioned, intermittent computing approaches can be classified as *static* and *reactive*. These two types of approaches fundamentally differs in how the load consumes power and makes forward progress, and hence, require different models for estimating forward progress.

IV. Modelling Reactive Intermittent Computing

We present a theoretical method to understand and model the forward progress in reactive intermittent computing given a constant current supply. This includes *Energy Storage* and *Intermittent Load* modules in the model framework. The

TABLE I
Model Parameters of Reactive Intermittent Computing

Input Parameters	
I_{harv}	Energy harvester current supply
C	Energy storage capacitance
Configuration Parameters	
I_{exe}	Execution current consumption
I_{sleep}	Sleep current consumption
I_r	Restore current consumption
I_s	Save current consumption
I_{leak}	Leakage current consumption
V_r	Restore voltage threshold
V_s	Save voltage threshold
T_r	Restore time overhead
T_s	Save time overhead
Output Parameter	
α_{exe}	Effective execution time ratio (forward progress)

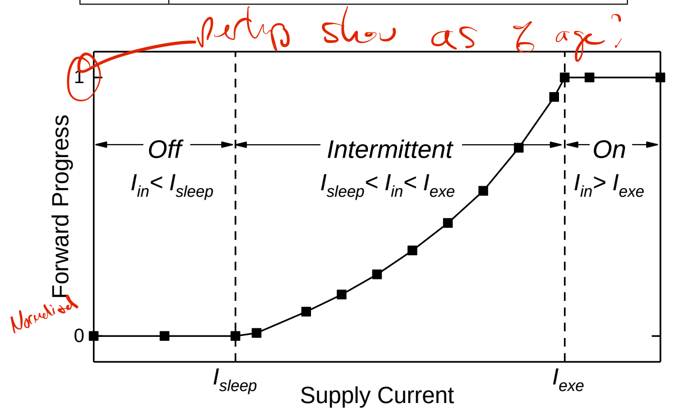

Fig. 2. Operating modes of reactive intermittent computing according to supply current and forward progress.

parameters of this model are listed in Table I. The model inputs, i.e. I_{harv} and C, are related to the size configuration of energy harvester and energy storage respectively. The model output is α_{exe}, the mean forward progress when a constant current supply is applied. In the model we assume that all the parameters maintains constant mean values.

We use I_{in} to denote usable current input for equation simplicity where:

$$I_{in} = I_{harv} - I_{leak} \tag{2}$$

The capacitor leakage effect is discussed at the end of in this section.

A. Operating Modes of Reactive Transient Computing

The behaviours of reactive intermittent computing can be classified as three operating modes given a spectrum of supply current. As shown in Fig. 2, an empirical experiment demonstrates the three operating modes. These three modes are divided by the relationship between the current input and current consumption. We denote the three modes as *Off*, *Intermittent*, and *On*.

Off mode: When $I_{in} < I_{sleep}$, the system cannot wake up. The supply voltage V_{cc} cannot be charged up to the restore threshold V_r to start execution, so the system stays inactive.

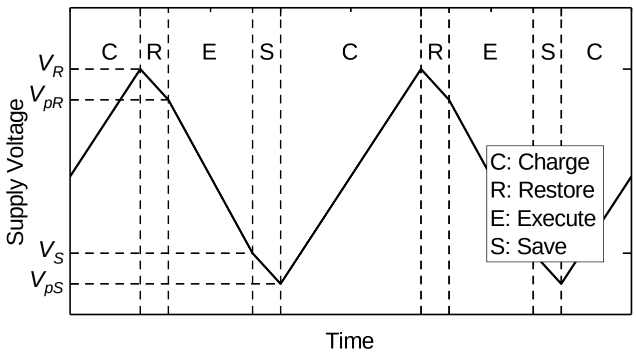

Fig. 3. Operating cycles in the Intermittent mode.

The sleep current I_{sleep} denotes the current consumption when the system waits for supply voltage to recover above the restore threshold, and hence, includes the consumption of voltage monitoring circuits.

Intermittent mode: When $I_{sleep} < I_{in} < I_{exe}$, the system executes when supply voltage is available intermittently. V_{cc} can be charged up to V_r and the system starts execution. However, the energy in energy storage is then consumed by the load as $I_{in} < I_{exe}$, causing V_{cc} to drop below the save threshold V_r, where the system saves its state and sleeps. The system sleeps until V_{cc} charges to V_r again and then resumes the execution. In general, higher I_{harv} leads to more forward progress in this mode, but the exact relationship between I_{harv} and forward progress requires further analysis.

On mode: When $I_{in} > I_{exe}$, the system execute constantly as the supply voltage V_{cc} never fails. The excess power either dissipates through circuits or overcharges V_{cc}. An overcharged V_{cc} may affect harvesting efficiency due to poor impedance matching and reduce I_{harv}, such that current input and consumption are in equilibrium.

B. Formulating Forward Progress

We aim to calculate how much forward progress is made in relation to energy storage capacity and current input through a theoretical analysis. In the following analysis, we focus on the Intermittent mode ($I_{sleep} < I_{in} < I_{exe}$), as the forward progress of the On mode and the Off mode is straightforward (i.e. 1 in the On mode and 0 in the Off mode).

In the Intermittent mode, as shown in Fig. 3, the system goes through four intervals in turn, i.e. charging, restoring, executing, and saving, with current consumption of I_{sleep}, I_r, I_{exe}, and I_s in each interval respectively.

Let V_{pr} (post-restore) and V_{ps} (post-save) denote the voltage after restoring and saving operations. V_{pr} and V_{ps} can be calculated as:

$$V_{pr} = V_r + \frac{T_r(I_{in} - I_r)}{C} \tag{3}$$

$$V_{ps} = V_s + \frac{T_s(I_{in} - I_s)}{C} \tag{4}$$

With Equation (3), the time spent on useful execution T_{exe} in one operating cycle can be expressed as:

$$\begin{aligned} T_{exe} &= \frac{C(V_{pr} - V_s)}{I_{exe} - I_{in}} \\ &= \frac{C(V_r - V_s) + T_r(I_{in} - I_r)}{I_{exe} - I_{in}} \end{aligned} \tag{5}$$

In Equation (5), $C(V_r - V_s)$ represents the amount of energy in the storage capacitor for restoring and executing. $T_r(I_{in} - I_r)$ represents the restoring cost. $I_{exe} - I_{in}$ is the current consumption for execution.

Also, with Equation (4), the charging interval can be described as:

$$\begin{aligned} T_{charge} &= \frac{C(V_r - V_{ps})}{I_{in} - I_{sleep}} \\ &= \frac{C(V_r - V_s) - T_s(I_{in} - I_s)}{I_{in} - I_{sleep}} \end{aligned} \tag{6}$$

Then, with Equation (5) and (6), the period of an operating cycle is:

$$\begin{aligned} T_{period} =& \quad T_{charge} + T_r + T_{exe} + T_s \\ =& \quad \frac{C(V_r - V_s) + T_s(I_{in} - I_s)}{I_{in} - I_{sleep}} + \\ & \quad \frac{C(V_r - V_s) + T_r(I_{exe} - I_r)}{I_{exe} - I_{in}} \end{aligned} \tag{7}$$

Finally, with T_{exe} and T_{period} calculated in Equation (5) and (7), we obtain the percentage of time spent on effective execution (forward progress) in the Intermittent mode:

$$\alpha_{exe} = \frac{T_{exe}}{T_{period}}, \quad I_{sleep} < I_{in} < I_{exe} \tag{8}$$

Higher α_{exe} leads to more time spent on forward progress. As $d\alpha_{exe}/dI_{in}$ is positive, higher harvested current I_{harv} leads to more forward progress. To find out the energy storage effect on α_{exe}, we need to analyze $d\alpha_{exe}/dC$. Here, if we assume the leakage current maintains constant when storage capacity increases, α_{exe} keeps increasing with C to approach $(I_{in} - I_{sleep})/(I_{exe} - I_{sleep})$, which is an ideal case where restore and save overheads are zero. However, in an electrolytic capacitor, the leakage current typically increases with storage capacity C in the following relationship:

$$I_{leak} = kCV_{cc} \tag{9}$$

where k is a constant normally in a range from 0.01 to 0.03 ($\frac{A}{F \cdot V}$). Therefore, referring to Equation (2), dI_{in}/dC is $-kV_{cc}$, which is negative. Hence, considering capacitor leakage increases with capacitance, there is an optimal capacity that leads to the maximum forward progress α_{exe}.

To include the Off and On modes, the forward progress given all supply levels is presented as:

$$\alpha_{exe} = \begin{cases} 0 & , \quad Off\,(I_{in} < I_{sleep}) \\ \dfrac{T_{exe}}{T_{period}} & , \quad Intermittent\,(I_{sleep} < I_{in} < I_{exe}) \\ 1 & , \quad On\,(I_{in} > I_{exe}) \end{cases} \tag{10}$$

where T_{exe} and T_{period} are calculated by Equation (5) and (7) respectively.

TABLE II
PROFILED MCU PARAMETERS

Parameter	Value
I_{exe}	887 µA
I_{sleep}	26 µA
I_r	971 µA
I_s	811 µA
T_r	1.903 ms
T_s	1.880 ms

V. EXPLORATION OF ENERGY STORAGE SIZING

A. Model Configuration

1) Energy Storage: The energy storage is represented as an ideal capacitor with current leakage. The terminal voltage of this buffering capacitor is directly applied to the load, so this capacitor is modelled as:

$$C\frac{dV_{cc}}{dt} = I_{harv} - I_{load} - I_{leak} \tag{11}$$

where I_{load} is the current consumption of the load. The leakage current I_{leak} in electrolytic capacitors demonstrates complex physical phenomenon. In the model exploration, we refer to an off-the-shelf tantalum capacitor [33], with an empirical I_{leak} in relation to capacitance C, rated voltage V_{rated}, and terminal voltage V_{cc} [34]:

$$I_{leak} = 0.01\lambda C V_{rated} \quad (A) \tag{12}$$

$$\lambda = 0.05 \times 20^{\frac{V_{cc}}{V_{rated}}} \tag{13}$$

where λ is ratio of the actual current leakage at V_{cc} to the current leakage at V_{rated}. V_{rated} is chosen to be 10 V so as to operate the load (typically $<$ 4.0 V) at 25–40 % of the rated voltage for low leakage design [34].

2) Load: We implemented and parameterized a reactive intermittent computing approach [14] on a TI MSP430FR6989 microcontroller. We profiled the model parameters by setting the MCU clock frequency at 8 MHz, running Dijkstra path finding algorithm with 1696B RAM usage in total. The supply voltage monitoring circuits use the MCU internal comparator and an external 3 MΩ voltage divider. The restore and save voltage thresholds are set as V_r = 2.4 V and V_s = 2.1 V respectively. The MCU shutdown voltage is V_{off} = 1.8 V.

The profiled parameters are shown in Table II. We measured the current consumption with a range of supply voltage. In experimental measurements, the variation of I_{sleep} between V_{off} and V_r is 2 %, and the variation of I_{exe} between V_s and 3.3 V is 1.5 %. I_{exe} also has a run-time variation of −2.4–2.8 % with constant supply voltage due to a variable memory access rate. We omit such negligible variations and use the mean of I_{exe} and I_{sleep} in the model. I_r and I_s are measured at V_r and V_s respectively. Given the voltage thresholds and the current consumption, the minimum energy storage to guarantee save and restore operations is 6.2 µF.

Although we define the parameters in the model, however, these parameters can be tuned to explore different load characteristics. For example, T_r and T_s can be tuned to model different volatile state sizes.

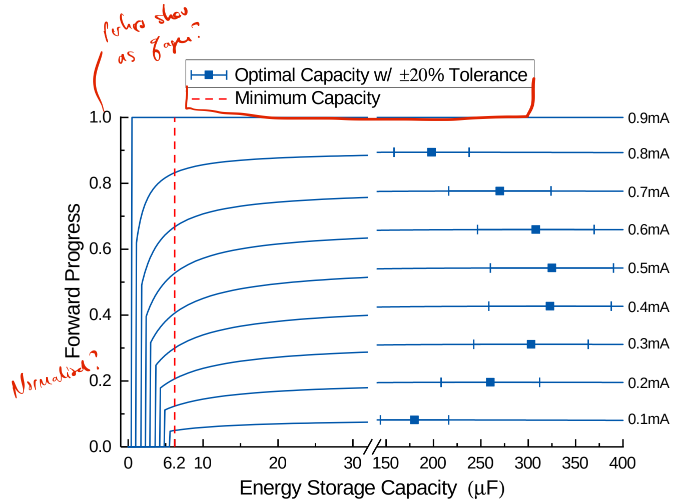

Fig. 4. Forward progress against energy storage capacity given different levels of constant supply current.

B. Sizing Energy Storage to Improve Forward Progress

1) Impact of Supply Current: Increasing energy storage capacity improves forward progress by prolonging the period of operating cycles and reducing the number of restore and save operations compared to the minimum energy storage. The relationship of forward progress and energy storage capacity is plotted given a range of constant current supply in Fig. 4. Forward progress increases as energy storage capacity increases beyond the minimum level (6.2 µF in this case). However, this improvement is offset by increased capacitor leakage, which leads to an optimal storage capacity.

When capacity is less than the minimum (in Fig. 4, the area on the left of the dashed line), the execution may still progress given that the current supply keeps providing energy during execution. However, if the restore or save operation cannot be completed even with the energy input during execution, the forward progress directly falls to zero as the volatile state cannot be preserved completely. This steep fall is because the implemented control algorithm enters the low-power mode with volatile state retained after a save operation, and hence, the energy used for restoring state in the first operating cycle is then used for effective execution in the following operating cycles as long as the supply voltage recovers to the restore threshold without a power failure (which is achieved with the constant current supply).

As a further illustration shown in Fig. 5, the maximum forward progress improvement, compared to using the minimum energy storage, can achieve up to 64.9 %with regard to a range of supply current. Typically, capacitors in manufacture has ±20 % tolerance of capacitance. This effect of capacitance variations on forward progress is also plotted in Fig. 4, where it is shown to be trivial ($<$ 0.23 % of the maximum values). Correspondingly, the optimal energy storage capacity is also plotted against supply current. It may not be preferable to optimise the energy storage capacitor with the sole goal of maximising forward progress because other concerns exist in increasing capacity, e.g. recharging time and dimensions (latter explained in Section VII-C). As we observe that the progress change is trivial around the optimal storage capacity, we also can't you write these out in full? More room, + font size is >> than body text..

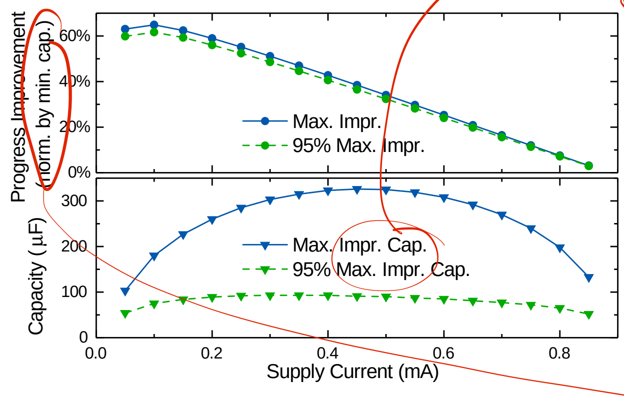

Fig. 5. Maximum forward progress improvement by sizing energy storage given a spectrum of supply current, with the corresponding optimal and sub-optimal (95 %of maximum improvement) capacitance.

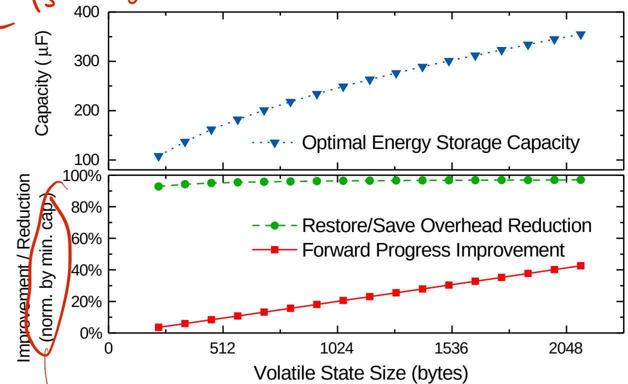

Fig. 6. Impact of RAM usage (linear to restore/save overhead) on sizing energy storage with 0.4 mA current supply.

Put in captions instead?

TABLE III
LINEAR SCALING RANGE OF VOLATILE STATE SIZE AND RESTORE/SAVE TIME OVERHEADS

State Size (Registers + SRAM)	Restore Time	Save Time
64B + 160B (lower bound)	232 µs	208 µs
64B + 2048B (upper bound)	2.298 ms	2.274 ms

plot in Fig. 5 the storage capacity which achieves 95 % of the maximum improvement, with a significant reduction of capacity (e.g. from 325 µF to 90 µF at 0.5 mA supply and 68.8 % mean capacity reduction).

2) Impact of Volatile State Size: The size of volatile state differs across different applications due to their different amounts of RAM usage, and hence, incurs application-specific time overheads for restore and save operations. Although the time overheads are profiled for one application, the model can be tuned to explore other applications with various volatile state sizes. We modelled the volatile state size variations by linearly scaling restore and save time overheads, as the time overheads of restore and save operations are linear to the size of volatile state [18]. We measured time overheads of restore and save operations in the minimum case (64B register data and a 160B stack) and the maximum case (64B register data and 2048B full RAM) respectively as shown in Table III.

An example of this exploration on volatile state size is plotted in Fig. 6 with 0.4 mA supply current. The forward progress improvement that can be gained from sizing energy storage increases with the volatile state size, and the optimal storage capacity grows accordingly. The improvement becomes insignificant when the volatile state size is small because the restore and save overheads are already negligible. For example, when the workload uses the least volatile state (the left end point in Fig. 6), the maximum progress improvement is only 3.6 % although the restore and save overheads are reduced by 92.9 %.

VI. MODEL VALIDATION

This section shows the comparison between the experimental and modelled forward progress to validate the proposed reactive intermittent computing model and the exploration results.

A. Experiment Setup

With the identical platform properties and workload settings in simulation setup, we used the TI MSP430FR6989 development board as the test platform. The on-board capacitance is measured to be 10.0 µF. This is the minimum capacitance that can be experimented on the platform. Additional capacitors were added to provide extra energy storage. The leakage current of these capacitors are less than 10 nA at 3 V, which is negligible compared to the current consumption of the platform (µA current draw), and hence, we omit the leakage of capacitors in the following experiment and model comparison.

In this practical experiment, the task completion rate (i.e. tasks completed per second) is used as the metric of forward progress rather than the effective execution time ratio. To gain the task completion rate from the model, we multiply the execution time ratio generated from our model by the completion rate when the device is executing constantly, since the task completion rate is linear to the effective execution time.

B. Results

1) Model Accuracy: To validate the accuracy of our model, we powered the device with a range of supply currents to operate the device in the Intermittent mode (0.1–0.8 mA, 0.1 mA per step), and repeated the tests with three energy storage capacities: a) on-board 10.0 µF capacitance only; b) 21.5 µF measured in total (11.5 µF added); c) 43.0 µF measured in total (33.0 µF added). We compared the actual forward progress with the one that our model generated. As shown in Fig. 7, the model generated output matches closely with the experimental results with only 0.5 %MAPE. Hence, the model is able to accurately estimate forward progress for design exploration.

2) Forward Progress Optimisation: We compared the tested completion speed among a theoretical minimum capacity case (6.2 µF, model generated), an on-board 10 µF, a 43 µF one suggested by the sizing process, and an ideal case. The ideal case

Not forward progress...?

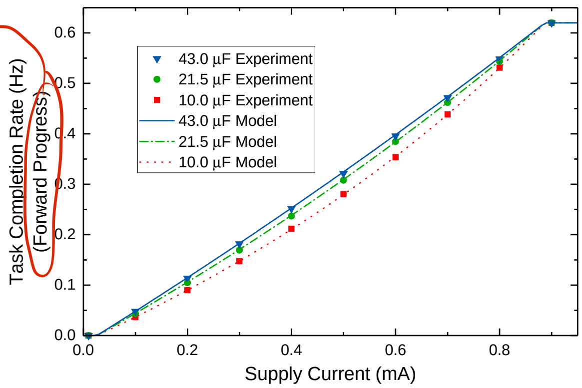

Fig. 7. Model validation by comparing the experimented and modelled task completion rates (forward progress) with different capacitance and supply current.

Log?

%

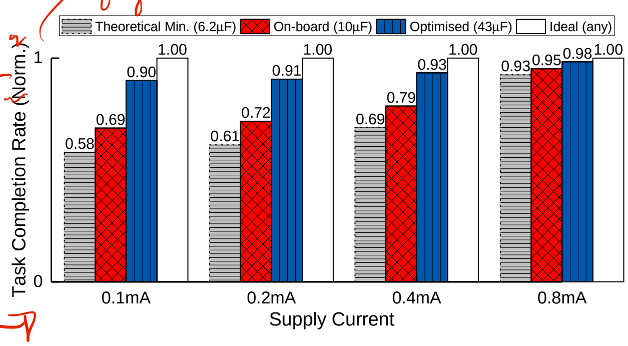

Fig. 8. Experimental comparison of task completion rates (forward progress) among different energy storage capacity.

switches between the sleep mode and the active mode without overheads of restoring and saving operations (mentioned in Section IV-B). As shown in Fig. 8, a reasonably sized energy storage capacity (43 µF) improves up to 55.2 % and 30.4 % more progress compared to the theoretical minimum capacitance and the platform on-board capacitance respectively, and also maintain at least 90 % of the ideal forward progress. The forward progress improvement by sizing energy storage is significant when supply is weak and relatively insignificant when supply is strong.

VII. Demonstration of Sizing Process

This section explains how this model framework is configured for design exploration in a PV-based EHIC device. Energy harvester and energy storage are modelled by existing models of PV cells and capacitors. We use a converter-less architecture where there is only a diode at the energy harvester output for preventing current backflow. The load is modelled by the forward progress formulation in Section IV-B, with parameters profiled on a TI MSP430FR6989 MCU. A diagram of the configured model is shown in Fig. 9.

A. Energy Source and Energy Harvester

We import NREL outdoor solar irradiance data [35] and EnHANTs indoor irradiance data [36] as the energy source conditions input. To convert irradiance to energy harvester

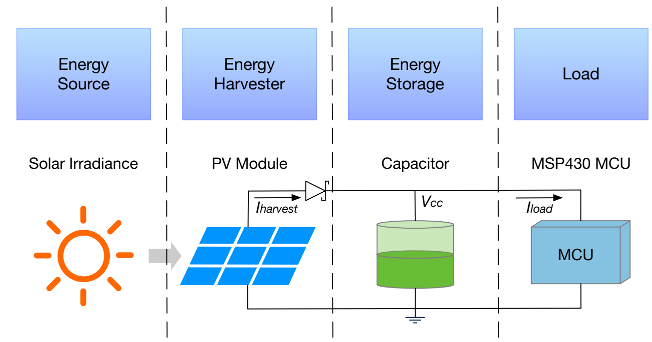

Fig. 9. Model configuration of a PV-based EHIC device.

TABLE IV
PV CELL MODEL PROPERTIES

Parameter	Value
Open-Circuit Voltage	0.89 V/cell
Short-Circuit Current	14.8 mA/cm^2
MPP Voltage	0.65 V/cell
MPP Current	12.1 mA/cm^2

power output, we adopt a datasheet-based PV cell model [37] developed recently. This model takes the parameters available in common PV cell datasheets, so it is easily reconfigured to suit different PV cells. According to this model, the output current I_o of a PV cell can be described as:

$$I_o = \frac{G}{G_{ref}} I_{sc}\left(1 - \left(1 - \frac{I_{mpp}}{I_{sc}}\right)^{\frac{V_o - V_{oc}}{V_{mpp} - V_{oc}}}\right) \tag{14}$$

where V_o is the output voltage of the PV cell, G is the ambient irradiance, G_{ref} is the reference irradiance (normally $1000W/m^2$), and I_{sc}, V_{oc}, I_{mpp}, V_{mpp} are respectively short-circuit current, open-circuit voltage, and the current and voltage at maximum power point (MPP) given the reference irradiance. V_o and G are dynamic at run time, while other parameters in this model are constant.

A PV panel is an array of PV cells, which amplifies voltage and current output by connecting PV cells in series or parallel. In a PV panel, the open-circuit voltage is proportional to the number of cells in series, and the short-circuit current is proportional to the area of each cell and the number of cells in parallel. We refer to a commercial solar cell [38] for PV cell properties as shown in Table IV. We set four cells in series (with V_{oc} = 3.56V) to match the operating voltage of the MCU (maximum 3.6V), and model energy harvester sizing by scaling the cell area. A Schottky diode is connected to the energy harvester output in order to prevent current backflow.

Before the simulation, we developed and explored two simulation processes: (a) simulate system state with a fine-grained time step, and (b) sort energy source conditions into a distribution in time lengths and process the distribution. Process (b) shows only 0.892 % MAPE compared to Process (a), while reducing simulation time significantly (e.g. from several hours to several seconds in a one-year test). Hence, we use Process (b) in the following tests.

B. Optimising Energy Storage in Deploying EHIC Devices under Real-World Energy Source Conditions

In the practical deployment of EHIC devices, ambient energy source conditions change over time and locations. The energy harvester and energy storage should be configured accordingly in order to achieve desired forward progress across various energy source conditions.

As a step of the sizing process, we use the aforementioned PV-based EHIC device model to find the PV panel area that achieves expected forward progress under different energy source conditions. To encompass different energy environments, four light source datasets across different environments are used in the following tests. To explore a range of target forward progress, three levels of minimum mean forward progress (i.e. target α_{exe}) are assumed to be 0.1, 0.2, and 0.3. We scale the PV panel area under the minimum energy storage to find the minimum PV panel area that achieves each target α_{exe}. As specified in Fig. 10, the energy harvester size that achieves desired forward progress may span over orders of magnitude given different energy source conditions (from mm^2 for outdoor sources to cm^2 for indoor sources).

We analyse the the sizing effect of energy storage on forward progress given real-world energy conditions. Fig. 10 shows 7.8–43.3 % mean forward progress improvement by sizing energy storage under real-world energy conditions. A takeaway is optimising energy storage can either improve forward progress upon a given energy harvester size, or reduce the energy harvester size that achieves the target forward progress. Given strong energy sources (e.g. Denver 2018 and Hawaii 2018 outdoor solar sources), increasing energy harvester size efficiently improves forward progress with minor dimensional overheads, e.g. tens of mm^2; however, given weak energy sources (e.g. EnHANTs Setup A and Setup D indoor light sources), optimising energy storage capacity save tens of cm^2 of PV panel area to achieve the same forward progress.

* Normalised? Show on figure?

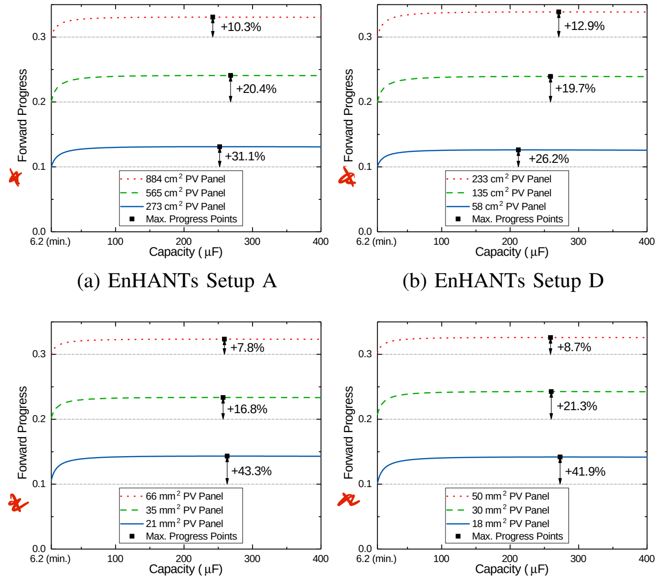

(a) EnHANTs Setup A (b) EnHANTs Setup D

(c) NREL Denver 2018 (d) NREL Hawaii 2018

Fig. 10. Forward progress improvement by sizing energy storage given different PV panel areas under real-world energy source conditions. The model is able to find the PV panel area required for achieving the target mean forward progress.

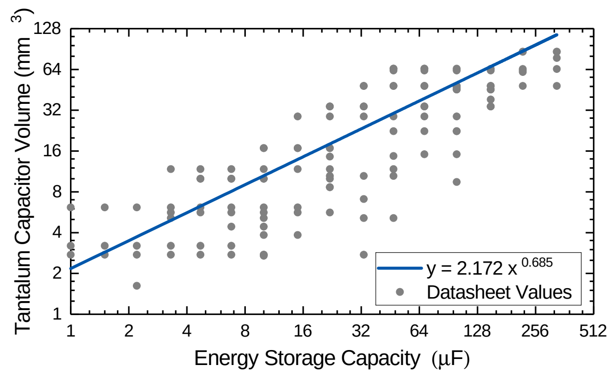

Fig. 11. Tantalum capacitor volume against capacitance [33], [39]–[43].

C. Trading off Forward Progress, Dimensions, and Recharging Time

Although increasing the storage capacity improves forward progress, larger capacitance may impact both dimensions and recharging time. We evaluate the overheads of increased capacitor dimensions and recharging time, and then trade off them with forward progress using a cost function to suggest an optimal capacitor size.

1) Metric of Dimensions: The overhead of capacitor dimensions is evaluated by characteristics of various off-the-shelf tantalum capacitors. We narrow down the range of sample capacitors within a set of characteristics: low-profile, 10V rated voltage, and Surface Mount Device (SMD) package, and select six series of capacitors [33], [39]–[43]. The volume and capacitance of these capacitors are plotted in Fig. 11 according to their datasheets. We use the regression of these data to represent the general capacitance-volume relationship in the sizing process.

2) Metric of Recharging Time: There is a recharging period between two consecutive execution periods in a intermittent computing device. During the recharging period, the device saves a volatile state, wait for supply voltage to recover, and restore the state to resume execution, without making forward progress. Applications that require frequent sensing may be negatively affected by such delay. We evaluate and consider this recharging time in our sizing process.

Technically, the actual recharging time between two active periods depends on capacitance, the start and end voltage of recharging, and the current input and consumption. While the end voltage (restore voltage) and current consumption can be set or predicted, the start voltage and current flows vary with energy source conditions. Instead of evaluating the recharging time in complex conditions, we use the time between two successive execution intervals given 0.5 mA supply current in the Intermittent mode as the metric of recharging time (or recharging ability). Using Equation (5) and (7), we can obtain this recharging period between two successive execution intervals in the Intermittent mode as:

$$
\begin{aligned}
T_{recharge} &= T_{period} - T_{exe} \\
&= \frac{C(V_r - V_s) + T_s(I_{in} - I_s)}{I_{in} - I_{sleep}} + T_r
\end{aligned} \tag{15}
$$

3) Trade-offs: From the previous observations (Fig. 5) we can see that to achieve the optimal progress improvement costs much more storage capacity (mean 3.2×) than to achieve 95 % improvement. A trade-off is necessary to improve progress while restricts the overheads of increased capacitor volume and recharging time.

As a part of the proposed sizing process, the cost function Equation (1) is used to trade off forward progress, capacitor volume, recharging time. We configure the function by setting $k_1 = 0.2$, $k_2 = 200$, and $k_3 = 1$, i.e.:

$$
f = \frac{\alpha_{exe}}{0.2} - (\frac{v_{cap}}{200})^2 - T_{recharge}^2 \tag{16}
$$

where v_{cap} is in mm^3 and $T_{recharge}$ is in second. k_1, k_2, and k_3 are scaling factors, and $\frac{1}{k_1}/\frac{1}{k_2} = 1000$ does not mean that forward progress is 1000 times more important than capacitor volume.

The effect of the trade-off is plotted in Fig. 12 using Denver 2018 energy source dataset as an example. On average, the sizing process of energy storage achieves 98.3 % of the maximum forward progress, while reduces 71.7 % capacitor volume and 83.8 % recharging time.

Compared to the minimum storage case, the sizing process improves mean forward progress by 5.7–25.3 % with energy storage increased from 6.2 µF to 36–46 µF (depending on PV panel area). According to Fig. 11, the closest available capacitance that ensures the minimum storage is 6.8 µF, whereas the closest available capacitance to achieve the optimal capacitance are 33 µF or 47 µF. The minimum volume for these three capacitance are 2.75 mm^3, 2.75 mm^3, and 5.12 mm^3, which means using the optimal capacitance, instead of the minimum one, may not incur dimensional overhead (for 33 µF). For 47 µF, the absolute volume (5.12 mm^3) is still insignificant compared to the device as a whole, e.g. an MSP430FR6989 MCU chip alone occupies 14 × 14 × 1.4mm^3 (274.4 mm^3). The regressed volume of the above three capacitance values are 8.1 mm^3, 23.8 mm^3, 30.4 mm^3 respectively. Again, such is still insignificant compared to the device as a whole.

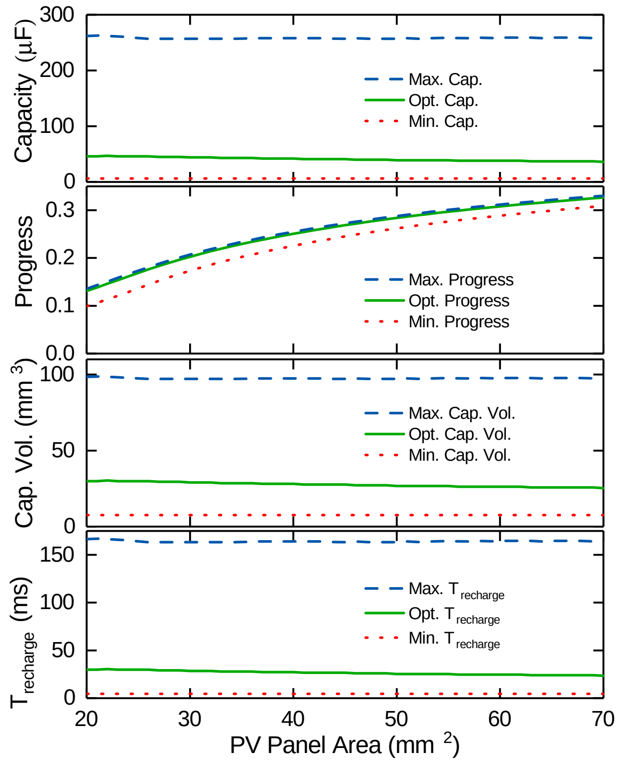

Fig. 12. The sizing process trades off forward progress, capacitor volume, and recharging time. The results are plotted against a range of PV panel area, given Denver 2018 energy source dataset.

VIII. Conclusion

In this paper, we proposed a model of reactive intermittent computing to estimate forward progress. Using this model, we explored the sizing effect of energy storage on forward progress in reactive intermittent computing with respect to supply current and volatile state size, showing up to 64.9 % progress improvement under constant current supply and 7.8–43.3 % improvement on annual mean forward progress under various real-world energy conditions. We proposed a process of sizing energy storage in deploying EHIC devices, which trades off forward progress, capacitor dimensions, and recharging time. We integrated the model into a PV-based EHIC device framework to demonstrate the sizing process, where results show that the suggested energy storage capacity achieves 98.3 % of the maximum forward progress while saving 71.7 % capacitor volume and 83.8 % recharging time. We validated the reactive intermittent computing model, which demonstrates only 0.5 % MAPE on forward progress compared to the experimentally measured values. Experimental results also showed that a reasonbly sized 43 µF capacitor improves forward progress by up to 55.2 % and 30.4 % compared to a theoretical minimum 6.2 µF one and an on-board 10 µF one across various levels of supply current. We believe that energy storage in intermittent systems should not be simply minimised or indiscriminately picked. Instead, the design of energy storage plays a significant role in practical deployment of EHIC devices.

References

[1] L. Mainetti, L. Patrono, and A. Vilei, "Evolution of wireless sensor networks towards the internet of things: A survey," in *SoftCOM 2011, 19th International Conference on Software, Telecommunications and Computer Networks*, Sep. 2011, pp. 1–6.

[2] O. Hahm, E. Baccelli, H. Petersen, and N. Tsiftes, "Operating systems for low-end devices in the internet of things: A survey," *IEEE Internet of Things Journal*, vol. 3, no. 5, pp. 720–734, Oct 2016.

[3] T. Adegbija, A. Rogacs, C. Patel, and A. Gordon-Ross, "Microprocessor optimizations for the internet of things: A survey," *IEEE Transactions on Computer-Aided Design of Integrated Circuits and Systems*, vol. 37, no. 1, pp. 7–20, Jan 2018.

[4] W. Shi, J. Cao, Q. Zhang, Y. Li, and L. Xu, "Edge computing: Vision and challenges," *IEEE Internet of Things Journal*, vol. 3, no. 5, pp. 637–646, Oct 2016.

[5] Sravanthi Chalasani and J. M. Conrad, "A survey of energy harvesting sources for embedded systems," in *IEEE SoutheastCon 2008*, April 2008, pp. 442–447.

Your referees can be shortened – shouldn't be taking up 5-6 lines each!

[6] S. Sudevalayam and P. Kulkarni, "Energy harvesting sensor nodes: Survey and implications," *IEEE Communications Surveys Tutorials*, vol. 13, no. 3, pp. 443–461, Third 2011.

[7] A. Kansal, J. Hsu, S. Zahedi, and M. B. Srivastava, "Power management in energy harvesting sensor networks," *ACM Trans. Embed. Comput. Syst.*, vol. 6, no. 4, Sep. 2007. [Online]. Available: http://doi.acm.org/10.1145/1274858.1274870

[8] B. Buchli, F. Sutton, J. Beutel, and L. Thiele, "Dynamic power management for long-term energy neutral operation of solar energy harvesting systems," in *Proceedings of the 12th ACM Conference on Embedded Network Sensor Systems*, ser. SenSys '14. New York, NY, USA: ACM, 2014, pp. 31–45. [Online]. Available: http://doi.acm.org/10.1145/2668332.2668333

[9] P. Wägemann, T. Distler, H. Janker, P. Raffeck, V. Sieh, and W. SchröDer-Preikschat, "Operating energy-neutral real-time systems," *ACM Trans. Embed. Comput. Syst.*, vol. 17, no. 1, pp. 11:1–11:25, Aug. 2017. [Online]. Available: http://doi.acm.org/10.1145/3078631

[10] X. Jiang, J. Polastre, and D. Culler, "Perpetual environmentally powered sensor networks," in *Proceedings of the 4th International Symposium on Information Processing in Sensor Networks*, ser. IPSN '05. Piscataway, NJ, USA: IEEE Press, 2005. [Online]. Available: http://dl.acm.org/citation.cfm?id=1147685.1147765

[11] F. Simjee and P. H. Chou, "Everlast: Long-life, supercapacitor-operated wireless sensor node," in *Proceedings of the 2006 International Symposium on Low Power Electronics and Design*, ser. ISLPED '06. New York, NY, USA: ACM, 2006, pp. 197–202. [Online]. Available: http://doi.acm.org/10.1145/1165573.1165619

[12] B. Ransford, J. Sorber, and K. Fu, "Mementos: System support for long-running computation on RFID-scale devices," in *Proceedings of the Sixteenth International Conference on Architectural Support for Programming Languages and Operating Systems*, ser. ASPLOS XVI. New York, NY, USA: ACM, 2011, pp. 159–170. [Online]. Available: http://doi.acm.org/10.1145/1950365.1950386

[13] H. Jayakumar, A. Raha, and V. Raghunathan, "QUICKRECALL: A low overhead HW/SW approach for enabling computations across power cycles in transiently powered computers," in *2014 27th International Conference on VLSI Design and 2014 13th International Conference on Embedded Systems*, Jan 2014, pp. 330–335.

[14] D. Balsamo, A. S. Weddell, G. V. Merrett, B. M. Al-Hashimi, D. Brunelli, and L. Benini, "Hibernus: Sustaining computation during intermittent supply for energy-harvesting systems," *IEEE Embedded Systems Letters*, vol. 7, no. 1, pp. 15–18, March 2015.

[15] B. Lucia and B. Ransford, "A simpler, safer programming and execution model for intermittent systems," in *Proceedings of the 36th ACM SIGPLAN Conference on Programming Language Design and Implementation*, ser. PLDI '15. New York, NY, USA: ACM, 2015, pp. 575–585. [Online]. Available: http://doi.acm.org/10.1145/2737924.2737978

[16] Y. Wang, Y. Liu, S. Li, D. Zhang, B. Zhao, M. Chiang, Y. Yan, B. Sai, and H. Yang, "A 3us wake-up time nonvolatile processor based on ferroelectric flip-flops," in *2012 Proceedings of the ESSCIRC (ESSCIRC)*, Sep. 2012, pp. 149–152.

[17] J. V. D. Woude and M. Hicks, "Intermittent computation without hardware support or programmer intervention," in *12th USENIX Symposium on Operating Systems Design and Implementation (OSDI 16)*. Savannah, GA: USENIX Association, Nov. 2016, pp. 17–32. [Online]. Available: https://www.usenix.org/conference/osdi16/technical-sessions/presentation/vanderwoude

[18] S. T. Sliper, D. Balsamo, N. Nikoleris, W. Wang, A. S. Weddell, and G. V. Merrett, "Efficient state retention through paged memory management for reactive transient computing," in *Proceedings of the 56th Annual Design Automation Conference 2019*, ser. DAC '19. New York, NY, USA: ACM, 2019, pp. 26:1–26:6. [Online]. Available: http://doi.acm.org/10.1145/3316781.3317812

[19] S. T. Sliper, O. Cetinkaya, A. S. Weddell, B. Al-Hashimi, and G. V. Merrett, "Energy-driven computing," *Philosophical Transactions of the Royal Society A: Mathematical, Physical and Engineering Sciences*, vol. 378, no. 2164, p. 20190158, 2020. [Online]. Available: https://royalsocietypublishing.org/doi/abs/10.1098/rsta.2019.0158

[20] K. Ma, X. Li, K. Swaminathan, Y. Zheng, S. Li, Y. Liu, Y. Xie, J. J. Sampson, and V. Narayanan, "Nonvolatile processor architectures: Efficient, reliable progress with unstable power," *IEEE Micro*, vol. 36, no. 3, pp. 72–83, May 2016.

[21] K. Ma, Y. Zheng, S. Li, K. Swaminathan, X. Li, Y. Liu, J. Sampson, Y. Xie, and V. Narayanan, "Architecture exploration for ambient energy harvesting nonvolatile processors," in *2015 IEEE 21st International Symposium on High Performance Computer Architecture (HPCA)*, Feb 2015, pp. 526–537.

[22] D. Balsamo, A. S. Weddell, A. Das, A. R. Arreola, D. Brunelli, B. M. Al-Hashimi, G. V. Merrett, and L. Benini, "Hibernus++: A self-calibrating and adaptive system for transiently-powered embedded devices," *IEEE Transactions on Computer-Aided Design of Integrated Circuits and Systems*, vol. 35, no. 12, pp. 1968–1980, 2016.

[23] D. Balsamo, A. Das, A. S. Weddell, D. Brunelli, B. M. Al-Hashimi, G. V. Merrett, and L. Benini, "Graceful performance modulation for power-neutral transient computing systems," *IEEE Transactions on Computer-Aided Design of Integrated Circuits and Systems*, vol. 35, no. 5, pp. 738–749, May 2016.

[24] J. Hester, L. Sitanayah, and J. Sorber, "Tragedy of the coulombs: Federating energy storage for tiny, intermittently-powered sensors," in *Proceedings of the 13th ACM Conference on Embedded Networked Sensor Systems*, ser. SenSys 15. New York, NY, USA: Association for Computing Machinery, 2015, p. 516. [Online]. Available: https://doi.org/10.1145/2809695.2809707

[25] D. Balsamo, B. J. Fletcher, A. S. Weddell, G. Karatziolas, B. M. Al-Hashimi, and G. V. Merrett, "Momentum: Power-neutral performance scaling with intrinsic mppt for energy harvesting computing systems," *ACM Trans. Embed. Comput. Syst.*, vol. 17, no. 6, Jan. 2019. [Online]. Available: https://doi.org/10.1145/3281300

[26] K. Maeng and B. Lucia, "Adaptive dynamic checkpointing for safe efficient intermittent computing," in *13th USENIX Symposium on Operating Systems Design and Implementation (OSDI 18)*. Carlsbad, CA: USENIX Association, Oct. 2018, pp. 129–144. [Online]. Available: https://www.usenix.org/conference/osdi18/presentation/maeng

[27] K. Maeng, A. Colin, and B. Lucia, "Alpaca: Intermittent execution without checkpoints," *Proc. ACM Program. Lang.*, vol. 1, no. OOPSLA, pp. 96:1–96:30, Oct. 2017. [Online]. Available: http://doi.acm.org/10.1145/3133920

[28] K. Maeng and B. Lucia, "Supporting peripherals in intermittent systems with just-in-time checkpoints," in *Proceedings of the 40th ACM SIGPLAN Conference on Programming Language Design and Implementation*, ser. PLDI 2019. New York, NY, USA: ACM, 2019, pp. 1101–1116. [Online]. Available: http://doi.acm.org/10.1145/3314221.3314613

[29] F. Su, Y. Liu, X. Sheng, H. G. Lee, N. Chang, and H. Yang, "A task failure rate aware dual-channel solar power system for nonvolatile sensor nodes," *ACM Trans. Embed. Comput. Syst.*, vol. 18, no. 4, pp. 33:1–33:21, Jul. 2019. [Online]. Available: http://doi.acm.org/10.1145/3320270

[30] J. San Miguel, K. Ganesan, M. Badr, and N. E. Jerger, "The EH model: Analytical exploration of energy-harvesting architectures," *IEEE Computer Architecture Letters*, vol. 17, no. 1, pp. 76–79, Jan 2018.

[31] J. San Miguel, K. Ganesan, M. Badr, C. Xia, R. Li, H. Hsiao, and N. Enright Jerger, "The EH model: Early design space exploration of intermittent processor architectures," in *2018 51st Annual IEEE/ACM International Symposium on Microarchitecture (MICRO)*, Oct 2018, pp. 600–612.

[32] N. Jackson, J. Adkins, and P. Dutta, "Capacity over capacitance for reliable energy harvesting sensors," in *Proceedings of the 18th International Conference on Information Processing in Sensor Networks*, ser. IPSN '19. New York, NY, USA: ACM, 2019, pp. 193–204. [Online]. Available: http://doi.acm.org/10.1145/3302506.3310400

[33] AVX, "AVX TAJ low profile series tantalum capacitors," http://datasheets.avx.com/TAJ_LOW_PROFILE.pdf, last accessed: 2 Dec, 2019.

[34] R. Faltus, "Low leakage current aspect of designing with tantalum and niobium oxide capacitors," https://www.avx.com/docs/techinfo/Low_Leakage_Current_Aspect_Designing_Tantalum_Niobium_Oxide_Capacitors.pdf, last accessed: 28 Jan, 2019.

[35] A. Andreas and T. Stoffel, "NREL solar radiation research laboratory (SRRL): Baseline measurement system (bms); golden, colorado (data)," *NREL Report NO.DA-5500-56488*, 1981.

[36] M. Gorlatova, A. Wallwater, and G. Zussman, "Networking low-power energy harvesting devices: Measurements and algorithms," *IEEE Transactions on Mobile Computing*, vol. 12, no. 9, pp. 1853–1865, Sep. 2013.

[37] S. Vergura, "A complete and simplified datasheet-based model of PV cells in variable environmental conditions for circuit simulation," *Energies*, vol. 9, no. 5, 2016. [Online]. Available: http://www.mdpi.com/1996-1073/9/5/326

[38] Panasonic, "Amorton amorphous silicon solar cells."

[39] AVX, "AVX TACmicrochip low profile series tantalum capacitors," http://datasheets.avx.com/TAC_LP.pdf, last accessed: 2 Dec, 2019.

[40] ——, "AVX F92 series tantalum capacitors," http://datasheets.avx.com/F92.pdf, last accessed: 2 Dec, 2019.
[41] Vishay, "Vishay 572D series tantalum capacitors," http://www.vishay.com/docs/40064/572d.pdf, last accessed: 2 Dec, 2019.
[42] ——, "Vishay 591D series tantalum capacitors," https://www.vishay.com/docs/40012/591d.pdf, last accessed: 2 Dec, 2019.
[43] ——, "Vishay 592D series tantalum capacitors," http://www.vishay.com/docs/40004/592d.pdf, last accessed: 2 Dec, 2019.

Jie Zhan Biography text here.

Alex S. Weddell Biography text here.

Geoff V. Merrett Biography text here.